Ca_2FeOsO_6/Sr_2FeOsO_6 superlattice: Multiferroicity above room temperature with giant hybrid-improper ferroelectric polarization and high photovoltaic efficiency

Paresh C. Rout and Udo Schwingenschlögl

Physical Science and Engineering Division (PSE), King Abdullah University of Science and Technology (KAUST), Thuwal 23955-6900, Saudi Arabia

(Received 5 February 2022; revised 18 February 2023; accepted 28 February 2023; published 15 March 2023)

Using first-principles calculations, the structure and electronic properties of the room-temperature ferrimagnetic Ca_2FeOsO_6/Sr_2FeOsO_6 superlattice are investigated. We show that the superlattice hosts hybrid-improper ferroelectricity despite the fact that bulk Sr_2FeOsO_6 realizes an $a^0a^0c^-$ tilting pattern of the O octahedra. The magnitude is comparable to that of conventional ferroelectric materials and is found to increase under both compressive and tensile strain. In contrast to competing superlattices, a ferrimagnetic critical temperature above room temperature is realized. An indirect-to-direct band-gap transition is observed between +1% and +2% strain, coming along with localization of the valence and conduction states on different transition-metal sublattices, which enables efficient electron-hole separation upon photoexcitation. The potential gradient due to the ferroelectric polarization supports the electron-hole separation and a spectroscopic limited maximum efficiency of 27% confirms excellent potential in solar cell applications. The tunable room-temperature ferroelectricity, high critical temperature of the ferrimagnetic ordering with high magnetization, and favorable photoabsorption properties of the Ca_2FeOsO_6/Sr_2FeOsO_6 superlattice open up a broad range of technological applications.

DOI: 10.1103/PhysRevB.107.094419

I. INTRODUCTION

Multiferroic materials [1–5] (coexistence of ferroelectricity and magnetism) are the subject of intensive research for the development of memory devices based on electrical writing and magnetic reading or vice versa. Of key interest are the discovery and design of materials that simultaneously possess high ferroelectric polarization and ferromagnetic [or ferrimagnetic (FiM)] ordering with high magnetization. However, it turns out that these features rarely coexist at room temperature [6–8]. For instance, the famous single-crystalline multiferroic $BiFeO_3$ possesses a high ferroelectric polarization at room temperature but the magnetization is low [9,10]. The double-perovskite Bi_2NiMnO_6 is ferroelectric up to 485 K but impractical for applications due to its low ferromagnetic critical temperature of 140 K [11]. Both $GaFeO_3$ [8] and the $BiFeO_3/LaFeO_3$ superlattice [12] combine room-temperature ferroelectricity with magnetoelectric coupling but suffer from low magnetization.

As the structural and chemical complexities enable flexible tuning of the material properties, ferroelectricity may be induced artificially in double-perovskites. The nonferroelectric double-perovskite oxides Ca_2FeOsO_6 and Sr_2FeOsO_6 are particularly appealing due to their high magnetic critical temperatures [13,14]. Although Ca_2FeOsO_6 adopts $P2_1/n$ symmetry, Sr_2FeOsO_6 switches between $P2_1/n$ and $I4/m$ symmetries under strain [15]. It is known that (001)-oriented $(ABO_3)/(A'BO_3)$ superlattices can exhibit hybrid-improper ferroelectricity when both ABO_3 and $A'BO_3$ adopt an $a^-a^-c^+$ tilting pattern of the O octahedra, induced by layer-dependent displacements of the A-site cations ("hybrid") as a by-product of octahedral rotations ("improper") [16–21]. The double-perovskite superlattices R_2NiMnO_6/La_2NiMnO_6 (R = Ce to Er) exhibit ferroelectricity and ferromagnetism, however, below room temperature [18]. For R = Ce the critical temperature approaches room temperature, but the ferroelectric polarization and magnetization are low. The highest ferroelectric polarization for R = Er (largest displacements of the Er cations due to the smallest ionic radius) comes along with a ferromagnetic critical temperature of only 165 K. To address these limitations, it is important to identify materials that combine large antipolar displacements of the A-site cations with a magnetic critical temperature above room temperature.

In this paper, we suggest a superlattice of perovskite oxides that provide these properties based on hybrid-improper ferroelectricity. Note that recent methodological developments enable layer-by-layer deposition of perovskite oxide superlattices with high quality [22]. We study the Ca_2FeOsO_6/Sr_2FeOsO_6 superlattice and show that it adopts $P2_1$ symmetry ($a^-a^-c^+$ tilting pattern of the O octahedra) under both compressive and tensile strains despite the fact that Sr_2FeOsO_6 favors $I4/m$ symmetry ($a^0a^0c^-$ tilting pattern of the O octahedra) under compressive strain [15]. We demonstrate hybrid-improper ferroelectric polarization and show that it can be enhanced from 8 $\mu C/cm^2$ without strain to 20 $\mu C/cm^2$ under +5% strain and to 17 $\mu C/cm^2$ under −5%

strain ($BaTiO_3$: 27 μC/cm^2 [23]). The magnetic critical temperature remains above room temperature under +5% strain and increases to 550 K under −5% strain. An indirect-to-direct band-gap transition at +2% strain with the valence and conduction states localized on different transition-metal sublattices enables efficient electron-hole separation and low recombination upon photoexcitation. The potential gradient due to the ferroelectric polarization supports the electron-hole separation.

We perform first-principles calculations by the QUANTUM-ESPRESSO package [24] using the Perdew-Burke-Ernzerhof generalized gradient approximation for the exchange-correlation functional. We account for the correlation effects in the 3d and 5d transition-metal orbitals by on-site Coulomb interactions [25] of the established literature values (5 eV for Fe and 2 eV for Os [26]). For the parent compounds, this methodology provides agreement with the experimental findings [26,27]. Spin-orbit coupling has no relevant impact on the structural and electronic properties of Ca_2FeOsO_6 [26] and Sr_2FeOsO_6 [27], and, for this reason, is neglected to reduce the computational cost. An energy cutoff of 90 Ry is used for the plane-wave expansion and an energy cutoff of 640 Ry for the augmentation charge. The Brillouin zone is integrated on an 8×8×6 k mesh in the structure optimization, on a 14×14×12 k mesh for evaluating the electronic properties, and on a 10×40×10 k mesh for determining the ferroelectric polarization by the Berry phase approach (in which we choose $P2_1/n$ Ca_2FeOsO_6 as a reference at each strain value [28]). All the k meshes are of Monkhorst-Pack type and carefully tested for convergence. The total energy convergence criterion is set to 10^{-8} Ry, and the Hellmann-Feynman force convergence criterion is set to 10^{-5} Ry/Bohr. The optical properties are calculated by the G_0W_0 approach and the Bethe-Salpeter equation to include excitonic effects, employing the Vienna *ab initio* simulation package [29].

We build Ca_2FeOsO_6/Sr_2FeOsO_6 superlattices with $P2_1/n$ or $I4/m$ symmetry starting from the $P2_1/n$ or $I4/m$ bulk structure of Ca_2FeOsO_6 (pseudocubic lattice parameter of 3.91 Å) by replacing one of the two CaO layers in a 20-atom supercell by a SrO layer as shown in Fig. 1(a). We have checked that a layered arrangement of the Ca^{2+} and Sr^{2+} ions is energetically favorable by 19 meV per formula unit. We mimic epitaxial strain ϵ by varying the in-plane lattice parameter as $a(\epsilon) = \sqrt{2}(1+\epsilon)\times 3.91$ Å. From a practical perspective, this strain can be achieved by the substrates previously used for La-doped Bi_2FeCrO_6 [30] due to the similar lattice parameter. We optimize the length and angle of the c lattice vector for each strain value simultaneously with the atomic positions, corresponding to (001) epitaxial growth. This procedure is executed for all the magnetic orderings shown in Fig. 1(b) and for both the $I4/m$ and the $P2_1/n$ symmetries to capture the lattice effect on the energetics.

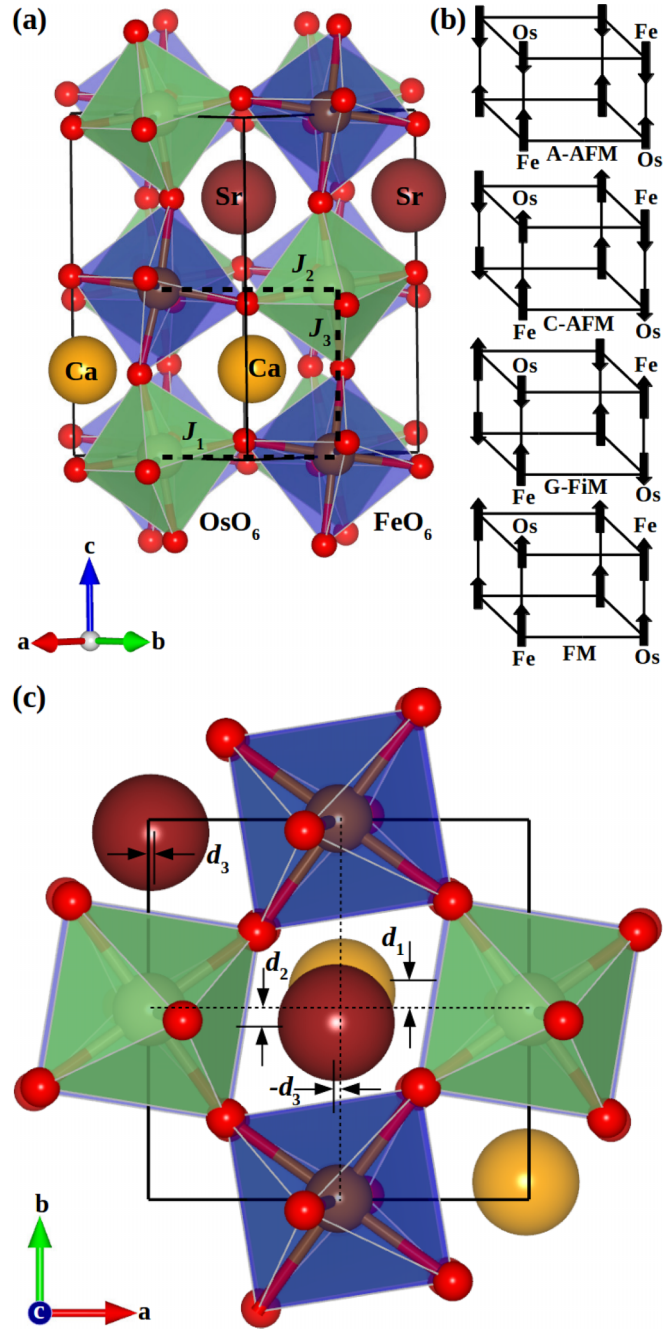

FIG. 1. (a) Ca_2FeOsO_6/Sr_2FeOsO_6 superlattice with exchange paths connecting the Fe and Os atoms, (b) considered magnetic orderings, and (c) antipolar displacements (d_1: Ca^{2+} along the b axis; d_2: Sr^{2+} along the b axis; d_3: Ca^{2+} along the a axis; $-d_3$: Sr^{2+} along the a axis).

II. RESULTS AND DISCUSSION

Figure 2 shows the obtained total energies with respect to the global minimum, indicating that the $P2_1/n$ symmetry with G-FiM ordering is favorable in the considered range of strain (and, therefore, will be studied in the following; see Fig. S1 in the Supplemental Material for the phonon band structure without strain [31]) despite the fact that Sr_2FeOsO_6 adopts $I4/m$ symmetry with C-antiferromagnetic (C-AFM) ordering under compressive strain [15] and Ca_2FeOsO_6 undergoes a transition from G-FiM ordering to C-AFM ordering at −5% strain and to E-AFM ordering at +5% strain. Interestingly, we always find an $a^-a^-c^+$ tilting pattern of the O octahedra, resembling Ca_2FeOsO_6, i.e., antiphase tilting of the FeO_6 and OsO_6 octahedra on the ab plane and in-phase tilting along the c axis, generating antipolar displacements of the Ca^{2+} and

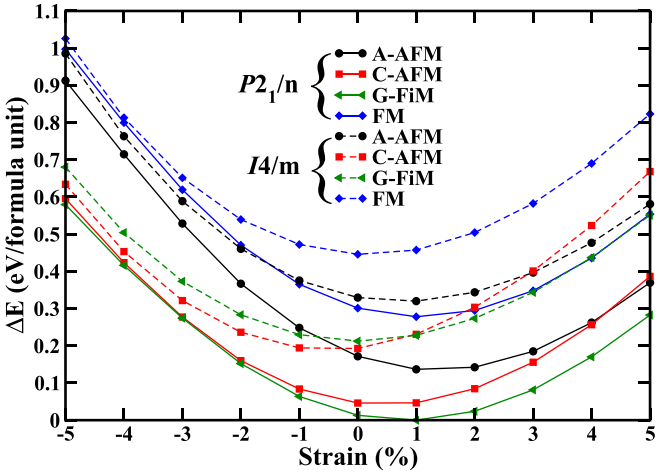

FIG. 2. Relative energies of the magnetic orderings as functions of the strain for the $P2_1/n$ (solid lines) and $I4/m$ (dashed lines) symmetries.

Sr^{2+} ions. It was argued that hybrid-improper ferroelectricity cannot emerge when one of the components of the superlattice

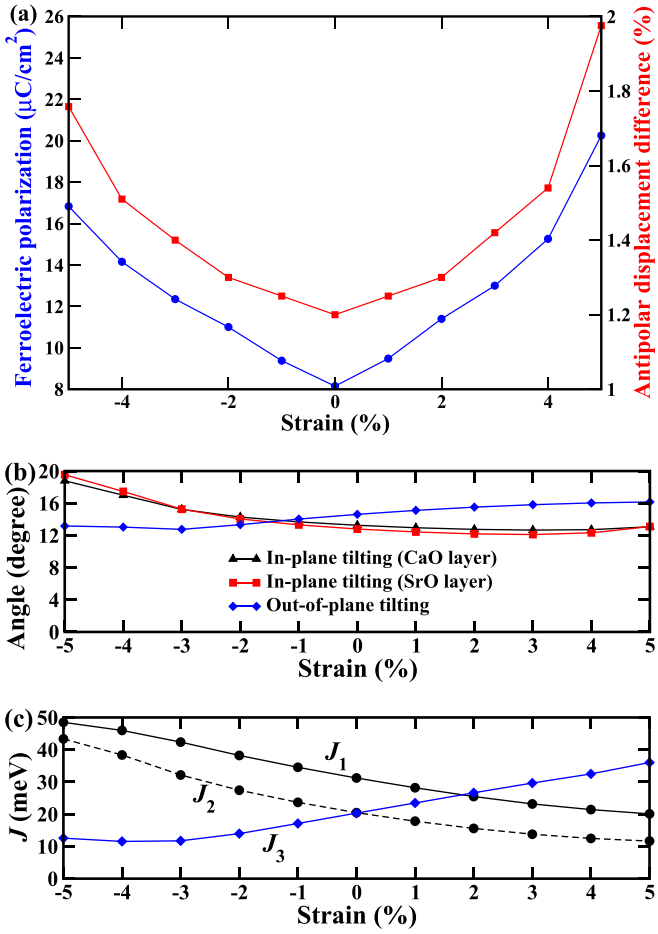

FIG. 3. (a) Ferroelectric polarization and difference between the antipolar displacements of the Sr^{2+} and Ca^{2+} ions (as a percentage of the lattice parameter), (b) tilting angles, and (c) magnetic coupling constants as functions of the strain.

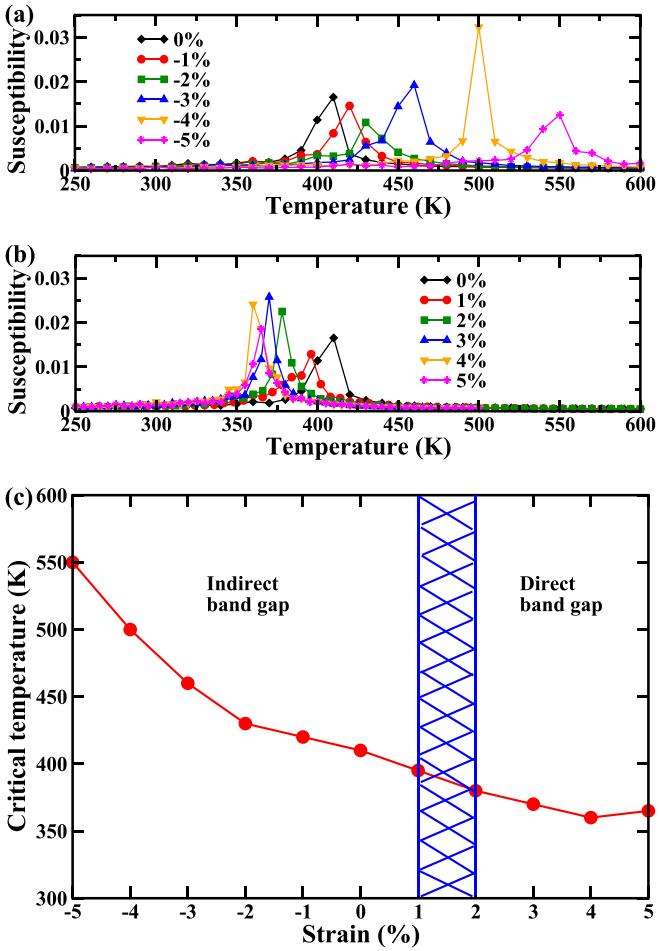

FIG. 4. Susceptibilities as functions of the temperature under (a) compressive and (b) tensile strains. The magnetic critical temperatures obtained from the peak positions are shown in (c) as a function of the expitaxial strain with the region of the indirect-to-direct band-gap transition marked.

adopts individually an $a^0a^0c^-$ tilting pattern of the O octahedra [17,18]. As Sr_2FeOsO_6 individually adopts this pattern, our findings invalidate the conjecture. The fact that the antipolar displacements (along the b axis) have different magnitudes, see Fig. 1, breaks the inversion symmetry and induces a finite ferroelectric polarization along the b axis. The displacements of nearest-neighbor Ca^{2+} ions and of nearest-neighbor Sr^{2+} ions are antipolar along the a axis, see Fig. 1, i.e., they do not result in ferroelectric polarization. Generally speaking, our findings indicate that there may exist also superlattices with hybrid-improper ferroelectricity based on components with other tilting patterns of the O octahedra if the tilting is modified in the superlattice.

We obtain for the ferroelectric polarization without strain a high value of 8 $\mu C/cm^2$ (see Fig. S2 in the Supplemental Material for the energy barrier to switch the direction [31]). The reason is that the radius of the Sr^{2+} ion is much larger than that of the isovalent Ca^{2+} ion. In contrast to Ref. [18], we find that the magnitude of the ferroelectric polarization is tuned significantly by strain, see Fig. 3(a). Interestingly, it increases both under compressive and tensile strains, reaching

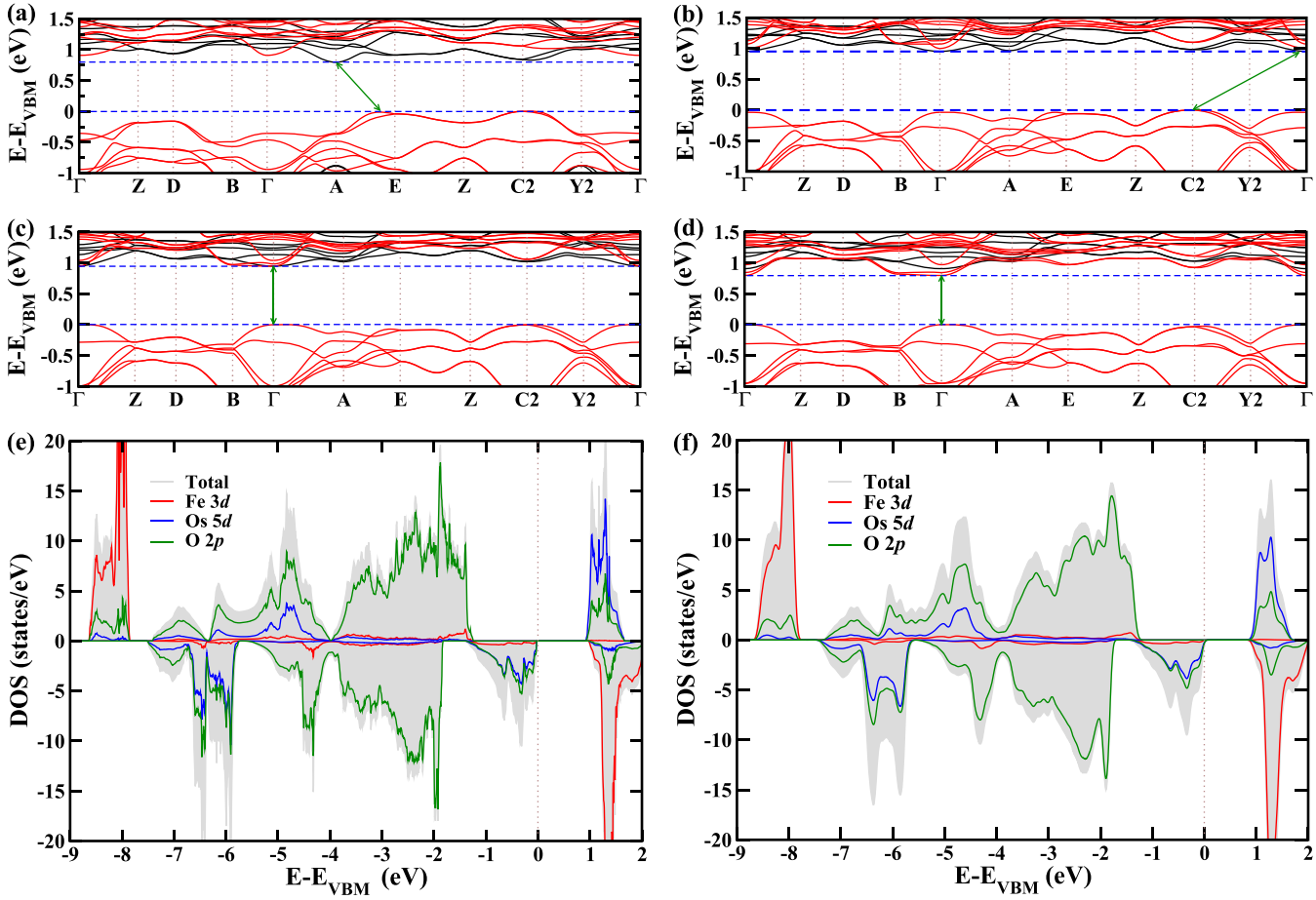

FIG. 5. Electronic band structures at (a) −5% (indirect band-gap), (b) 0% (indirect band-gap), (c) +2% (direct band-gap), and (d) +5% (direct band-gap) strain. The dashed lines mark the conduction-band minimum and valence-band maximum. Black and red colors represent the spin-up and spin-down channels, respectively. Densities of states at (e) 0% and (f) +2% strain.

20 μC/cm^2 at +5% strain and 17 μC/cm^2 at −5% strain. These values are much larger than predicted for the R_2NiMnO$_6$/La$_2$NiMnO$_6$ (R = Ce to Er) [18] and BiFeO$_3$/LaFeO$_3$ [12] superlattices, being comparable to those of conventional ferroelectric materials, such as BaTiO$_3$. To explain the increase inthe ferroelectric polarization under strain, we study the difference between the antipolar displacements of the Ca^{2+} and Sr^{2+} ions [$d_2 - d_1$; see Fig. 1(c)]. Figure 3(a) shows that it increases under both compressive and tensile strains similar to the ferroelectric polarization. Therefore, the different responses of the Ca^{2+} and Sr^{2+} ions to the strain explain the observed trend. According to Fig. 3(b), the antipolar displacements are enhanced under compressive and tensile strains due to enhanced in-plane and out-of-plane octahedral tiltings, respectively. We find no coupling between the ferroelectricity and the magnetism.

Since the parent compounds realize octahedral tiltings at room temperature [13,14,32], the Ca$_2$FeOsO$_6$/Sr$_2$FeOsO$_6$ superlattice will be ferroelectric at room temperature. To become a multiferroic material, however, it also has to exhibit magnetization. We find for the G-FiM ordering a magnetization of $2\mu_B$ per formula unit. To determine and understand the evolution of the magnetic critical temperature under strain, we next extract the magnetic coupling constants using a Heisenberg spin Hamiltonian $H = \sum_{ij} J_{ij}\vec{S}_i \cdot \vec{S}_j$, where J_{ij} is the coupling constant between sites i and j, and $\vec{S}_i$ and $\vec{S}_j$ are the spin vectors. We consider the in-plane nearest-neighbor couplings (J_1 and J_2) and the out-of-plane nearest-neighbor coupling (J_3), see Fig. 1(a). When we assume that the spin vectors are collinear with $|\vec{S}_i| = 1$ as the real magnitude later will be taken into account by Monte Carlo simulations, we can compute the magnetic coupling constants by solving the coupled equations $E_1 = E_0 + 4J_1 + 4J_2 - 4J_3$ (A-AFM), $E_2 = E_0 - 4J_1 - 4J_2 + 4J_3$ (C-AFM), $E_3 = E_0 - 4J_1 - 4J_2 - 4J_3$ (G-FiM), $E_4 = E_0 + 4J_1 + 4J_2 + 4J_3$ (FM), $E_5 = E_0 - 4J_1 + 4J_2$ (G-FiM with one Os spin flipped), and $E_6 = E_0 + 4J_1 - 4J_2$ (G-FiM with one Fe spin flipped), where E_0 is the lattice energy and E_1–E_6 are obtained as total energies from the first-principles calculations. According to Fig. 3(c), both nearest-neighbor coupling constants are always positive. This is due to the fact that the magnetic moments of the Fe and Os ions interact by AFM superexchange in both the in-plane (Fe-O-Os angles: 147°–153°) and out-of-plane (Fe-O-Os angles: 142°–153°) directions as per the Goodenough-Kanamori rules [33–36] and in agreement with our finding that the G-FiM ordering is energetically favorable. Note that the J_3 curve in Fig. 3(c) resembles the behavior of the out-of-plane tilting angle in Fig. 3(b).

We employ Monte Carlo simulations with Gaussian moves [37] for a 12×12×12 spin lattice, using 100 000 sweeps for the thermalization and 80 000 additional sweeps for the data generation. Without strain, we obtain a magnetic critical temperature of 420 K, which is significantly higher than the 350 K predicted for Ca_2FeOsO_6 and the 160 K predicted for Sr_2FeOsO_6. In Fig. 4, we show the magnetic critical temperature as a function of the strain. Interestingly, the values remain above room temperature, in contrast to findings for the R_2NiMnO_6/La_2NiMnO_6 (R = Ce to Er) superlattices [18]. They increase (decrease) under compressive (tensile) strain due to the increasing (decreasing) J_1 and J_2 despite the opposite trend of J_3, compare Fig. 3(c). Therefore, strain turns out to be a viable tool for tuning the magnetic critical temperature, letting the Ca_2FeOsO_6/Sr_2FeOsO_6 superlattice emerge as a room-temperature multiferroic material with immediate technological relevance.

Electronic band structures and densities of states at different strains are shown in Fig. 5. We observe a semiconducting state with an indirect-to-direct band-gap transition between +1% and +2% strains. The Fe and Os atoms adopt 3+ ($t_{2g}^3 e_g^2$) and 5+ ($t_{2g}^3 e_g^0$) states, respectively, in a high-spin configuration with the spins aligned antiparallel in both the in-plane and out-of-plane directions, which explains the magnetization of $2\mu_B$ per formula unit. In the spin-down channel (which forms the direct band-gap) the valence-band edge is dominated by hybridized O $2p$ and Os $5d$ states, whereas the conduction-band edge is almost entirely due to Fe-$3d$ states (see Fig. S3 in the Supplemental Material for the spatial distribution of the charge density [31]). As a consequence, similar to Bi_2FeCrO_6 [38], photoexcitation will lead to spatial electron-hole separation between the Fe and the Os sublattices, implying low recombination (as desired for photovoltaics) due to vanishing transition matrix elements. The ferroelectric polarization further reduces the recombination and, thus, supports the extraction of the photogenerated carriers [39,40].

The photoabsorption spectrum

$$\alpha(\omega) = \frac{\sqrt{2}\omega}{c}\sqrt{\sqrt{[\mathrm{Re}\,\epsilon(\omega)]^2 + [\mathrm{Im}\,\epsilon(\omega)]^2} - \mathrm{Re}\,\epsilon(\omega)},$$

where ω is the frequency and c is the speed of light, is determined taking into account excitonic effects through the Bethe-Salpeter equation. Comparing results at 0% (indirect band-gap) and +2% (direct band-gap) strains, Figure 6(a) shows that the low-energy absorption peak, which falls into the visible range, shifts slightly to the red under tensile strain. To predict the power conversion efficiency, we calculate the spectroscopic limited maximum efficiency, which depends on $\alpha(\omega)$, the nature of the band-gap, and the absorber thickness. The results are shown in Fig. 6(b) as a function of the absorber thickness. Interestingly, we find very high values of 25% and 27% (outperforming hybrid perovskites [41]) at 0% and +2% stain, respectively, confirming the excellent potential of the Ca_2FeOsO_6/Sr_2FeOsO_6 superlattice in solar energy harvesting.

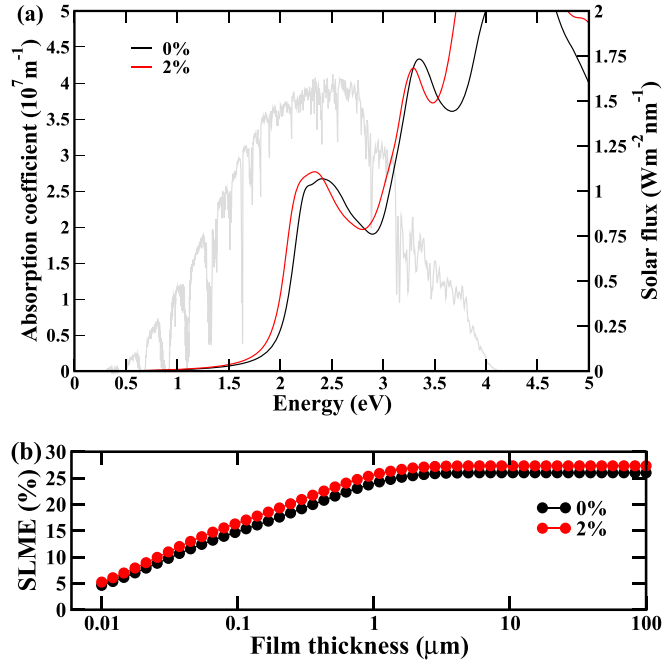

FIG. 6. (a) Photoabsorption spectrum (the gray curve is the AM 1.5G solar flux) and (b) spectroscopic limited maximum efficiency as function of the absorber thickness.

In conclusion, we predict a room-temperature multiferroic superlattice composed of the double-perovskite oxides Ca_2FeOsO_6 and Sr_2FeOsO_6. The superlattice exhibits ferroelectric polarization even though Sr_2FeOsO_6 individually adopts an $a^0a^0c^-$ tilting pattern of the O octahedra. We find antipolar displacements of the A-site cations in excess of those reported for the R_2NiMnO_6/La_2NiMnO_6 (R = Ce to Er) superlattices, which is due to a large difference in the radii of the Ca^{2+} and Sr^{2+} ions. The resulting hybrid-improper ferroelectric polarization increases both under compressive and tensile strains, reaching a magnitude comparable to that of conventional ferroelectric materials. Our calculations reveal that the ferroelectric polarization and magnetic critical temperature can be viably tuned by strain. The FiM ordering (finite magnetization) with high critical temperature is promising for room-temperature spintronics and data storage. In addition, the creation of a direct band-gap under tensile strain in combination with electron-hole separation between the Fe and Os sublattices opens up potential in photovoltaics. The ferroelectric polarization is beneficial for the extraction of the photogenerated carriers by supporting the electron-hole separation.

ACKNOWLEDGMENTS

The research reported in this publication was supported by funding from King Abdullah University of Science and Technology (KAUST). For computer time, this research used the resources of the Supercomputing Laboratory at KAUST.

[1] S. Cheong and M. Mostovoy, Multiferroics: A magnetic twist for ferroelectricity, Nat. Mater. **6**, 13 (2007).

[2] R. Ramesh and N. A. Spaldin, Multiferroics: Progress and prospects in thin films, Nat. Mater. **6**, 21 (2007).

[3] J. van den Brink and D. I. Khomskii, Multiferroicity due to charge ordering, J. Phys.: Condens. Matter **20**, 434217 (2008).

[4] S. Picozzi and C. Ederer, First principles studies of multiferroic materials, J. Phys.: Condens. Matter **21**, 303201 (2009).

[5] Y. Tokura and S. Seki, Multiferroics with Spiral spin orders, Adv. Mater. **22**, 1554 (2010).

[6] W. Eerenstein, N. D. Mathur, and J. F. Scott, Multiferroic and magnetoelectric materials, Nature (London) **442**, 759 (2006).

[7] Q. He, Y. H. Chu, J. T. Heron, S. Y. Yang, W. I. Liang, C. Y. Kuo, H. J. Lin, P. Yu, C. W. Liang, R. J. Zeches, W. C. Kuo, J. Y. Juang, C. T. Chen, E. Arenholz, A. Scholl, and R. Ramesh, Electrically controllable spontaneous magnetism in nanoscale mixed phase multiferroics, Nat. Commun. **2**, 225 (2011).

[8] S. Mukherjee, A. Roy, S. Auluck, R. Prasad, R. Gupta, and A. Garg, Room Temperature Nanoscale Ferroelectricity in Magnetoelectric $GaFeO_3$ Epitaxial Thin Films, Phys. Rev. Lett. **111**, 087601 (2013).

[9] J. Wang, J. B. Neaton, H. Zheng, V. Nagarajan, S. B. Ogale, B. Liu, D. Viehland, V. Vaithyanathan, D. G. Schlom, U. V. Waghmare, N. A. Spaldin, K. M. Rabe, M. Wuttig, and R. Ramesh, Epitaxial $BiFeO_3$ multiferroic thin film heterostructures, Science **299**, 1719 (2003).

[10] D. Albrecht, S. Lisenkov, W. Ren, D. Rahmedov, I. A. Kornev, and L. Bellaiche, Ferromagnetism in multiferroic $BiFeO_3$ films: A first-principles-based study, Phys. Rev. B **81**, 140401(R) (2010).

[11] M. Azuma, K. Takata, T. Saito, S. Ishiwata, Y. Shimakawa, and M. Takano, Designed ferromagnetic, ferroelectric Bi_2NiMnO_6, J. Am. Chem. Soc. **127**, 8889 (2005).

[12] Z. Zanolli, J. C. Wojdeł, J. Íñiguez, and P. Ghosez, Electric control of the magnetization in $BiFeO_3/LaFeO_3$ superlattices, Phys. Rev. B **88**, 060102(R) (2013).

[13] A. K. Paul, M. Jansen, B. Yan, C. Felser, M. Reehuis, and P. M. Abdala, Synthesis, crystal structure, and physical properties of Sr_2FeOsO_6, Inorg. Chem. **52**, 6713 (2013).

[14] H. L. Feng, M. Arai, Y. Matsushita, Y. Tsujimoto, Y. Guo, C. I. Sathish, X. Wang, Y. H. Yuan, M. Tanaka, and K. Yamaura, High-temperature ferrimagnetism driven by lattice distortion in double perovskite Ca_2FeOsO_6, J. Am. Chem. Soc. **136**, 3326 (2014).

[15] P. C. Rout and U. Schwingenschlögl, Strain-attenuated spin frustration in double perovskite Sr_2FeOsO_6, Phys. Rev. B **103**, 024426 (2021).

[16] N. A. Benedek and C. J. Fennie, Hybrid Improper Ferroelectricity: A Mechanism for Controllable Polarization-Magnetization Coupling, Phys. Rev. Lett. **106**, 107204 (2011).

[17] J. M. Rondinelli and C. J. Fennie, Octahedral rotation-induced ferroelectricity in cation ordered perovskites, Adv. Mater. **24**, 1961 (2012).

[18] H. J. Zhao, W. Ren, Y. Yang, J. Íñiguez, X. M. Chen, and L. Bellaiche, Near room-temperature multiferroic materials with tunable ferromagnetic and electrical properties, Nat. Commun. **5**, 4021 (2014).

[19] H. J. Zhao, J. Íñiguez, W. Ren, X. M. Chen, and L. Bellaiche, Atomistic theory of hybrid improper ferroelectricity in perovskites, Phys. Rev. B **89**, 174101 (2014).

[20] X. Q. Liu, J. W. Wu, X. X. Shi, H. J. Zhao, H. Y. Zhou, R. H. Qiu, W. Q. Zhang, and X. M. Chen, Hybrid improper ferroelectricity in ruddlesden-popper $Ca_3(Ti, Mn)_2O_7$ ceramics, Appl. Phys. Lett. **106**, 202903 (2015).

[21] Y. S. Oh, X. Luo, F.-T. Huang, Y. Wang, and S.-W. Cheong, Experimental demonstration of hybrid improper ferroelectricity and the presence of abundant charged walls in $(Ca, Sr)_3Ti_2O_7$ crystals, Nat. Mater. **14**, 407 (2015).

[22] Q. Lei, M. Golalikhani, B. A. Davidson, G. Liu, D. G. Schlom, Q. Qiao, Y. Zhu, R. U. Chandrasena, W. Yang, A. X. Gray, E. Arenholz, A. K. Farrar, D. A. Tenne, M. Hu, J. Guo, R. K. Singh, and X. Xi, Constructing oxide interfaces and heterostructures by atomic layer-by-layer laser molecular beam epitaxy, npj Quantum Mater. **2**, 10 (2017).

[23] W. Zhong, D. Vanderbilt, and K. M. Rabe, Phase Transitions in $BaTiO_3$ from First Principles, Phys. Rev. Lett. **73**, 1861 (1994).

[24] P. Giannozzi, S. Baroni, N. Bonini, M. Calandra, R. Car, C. Cavazzoni, D. Ceresoli, G. L. Chiarotti, M. Cococcioni, I. Dabo, A. D. Corso, S. D. Gironcoli, S. Fabris, G. Fratesi, R. Gebauer, U. Gerstmann, C. Gougoussis, A. Kokalj, M. Lazzeri, L. Martin-Samos *et al.*, QUANTUM ESPRESSO: A modular and open-source software project for quantum simulations of materials, J. Phys.: Condens. Matter **21**, 395502 (2009).

[25] V. I. Anisimov, F. Aryasetiawan, and A. I. Liechtenstein, First-principles calculations of the electronic structure and spectra of strongly correlated systems: The LDA+U method, J. Phys.: Condens. Matter **9**, 767 (1997).

[26] H. Wang, S. Zhu, X. Ou, and H. Wu, Ferrimagnetism in the double perovskite Ca_2FeOsO_6: A density functional study, Phys. Rev. B **90**, 054406 (2014).

[27] S. Kanungo, B. Yan, M. Jansen, and C. Felser, Ab initio study of low-temperature magnetic properties of double perovskite Sr_2FeOsO_6, Phys. Rev. B **89**, 214414 (2014).

[28] R. D. King-Smith and D. Vanderbilt, Theory of polarization of crystalline solids, Phys. Rev. B **47**, 1651 (1993).

[29] G. Kresse and D. Joubert, From ultrasoft pseudopotentials to the projector augmented-wave method, Phys. Rev. B **59**, 1758 (1999).

[30] A. Khare, A. Singh, S. S. Prabhu, and D. S. Rana, Controlling magnetism of multiferroic $(Bi_{0.9}La_{0.1})_2FeCrrO_6$ thin films by epitaxial and crystallographic orientation strain, Appl. Phys. Lett. **102**, 192911 (2013).

[31] See Supplemental Material at http://link.aps.org/supplemental/10.1103/PhysRevB.107.094419 for the phonon band structure without strain, total energy variation as a function of the ferroelectric distortion, and spatial distributions of the charge density at the VBM and CBM under +2% strain,

[32] A. K. Paul, M. Reehuis, V. Ksenofontov, B. Yan, A. Hoser, D. M. Többens, P. M. Abdala, P. Adler, M. Jansen, and C. Felser, Lattice Instability and Competing Spin Structures in the Double Perovskite Insulator Sr_2FeOsO_6, Phys. Rev. Lett. **111**, 167205 (2013).

[33] J. B. Goodenough, Theory of the role of covalence in the perovskite-type manganites [La, M(II)]MnO_3, Phys. Rev. **100**, 564 (1955).

[34] J. Kanamori, Superexchange interaction and symmetry properties of electron orbitals, J. Phys. Chem. Solids **10**, 87 (1959).

[35] E. O. Wollan, Magnetic coupling in crystalline compounds. A phenomenological theory of magnetism in 3d metals, Phys. Rev. **117**, 387 (1960).

[36] J. B. Goodenough, *Magnetism and Chemical Bond: Electronic Structure, Exchange and Magnetism in Oxides* (Interscience, New York, 1963).

[37] R. F. L. Evans, W. J. Fan, P. Chureemart, T. A. Ostler, M. O. A. Ellis, and R. W. Chantrell, Atomistic spin model simulations of magnetic nanomaterials, J. Phys.: Condens. Matter **26**, 103202 (2014).

[38] D. Kim, H. Han, J. H. Lee, J. W. Choi, J. C. Grossman, H. M. Jang, and D. Kim, Electron-hole separation in ferroelectric oxides for efficient photovoltaic responses, Proc. Natl. Acad. Sci. USA **115**, 6566 (2018).

[39] E. Assmann, P. Blaha, R. Laskowski, K. Held, S. Okamoto, and G. Sangiovanni, Oxide Heterostructures for Efficient Solar Cells, Phys. Rev. Lett. **110**, 078701 (2013).

[40] A. Quattropani, A. S. Makhort, M. V. Rastei, G. Versini, G. Schmerber, S. Barre, A. Dinia, A. Slaoui, J.-L. Rehspringer, T. Fix, S. Colis, and B. Kundys, Tuning photovoltaic response in Bi_2FeCrO_6 films by ferroelectric poling, Nanoscale **10**, 13761 (2018).

[41] J. Qian, B. Xu, and W. Tian, A comprehensive theoretical study of halide perovskites ABX_3, Org. Electron. **37**, 61 (2016).